RSC Advances

PAPER

Cite this: *RSC Adv.*, 2015, **5**, 71796

Grape-like mesostructured silica nanoparticle-decorated single-walled carbon nanotubes: silica growth and dye adsorptivity†

A. A. Jalil,*[ab] S. Triwahyono,[c] A. H. Karim,[c] N. K. Nordin,[b] U. A. Asli,[ab] M. H. Hassim[ab] and D. Prasetyoko[d]

Single-walled carbon nanotube (SWCNT)-mesostructured silica nanoparticle (MSN) adsorbents (S-MSNs) were prepared through a simple one-step method with various loadings of SWCNTs. Their surface properties were characterized by XRD, TEM, N_2 physisorption, and FTIR spectroscopy. A grape-like S-MSN was produced, for which the growth of MSNs became intense with increasing CNT loading. A bimodal pore structure also developed, which increased the average pore size and pore volume, but decreased the surface area. The increasing amount of CNTs was found to provide more sites for silica growth that enhanced the adsorptivity of the S-MSNs toward methylene blue (MB) dye. Accordingly, 0.1 g L^{-1} 5 wt% S-MSN was able to adsorb 478 mg g^{-1} (q_m) of 50 mg L^{-1} MB at pH 7 and 323 K. The equilibrium data were evaluated using the Langmuir, Freundlich, Redlich–Peterson, and Dubinin–Radushkevich isotherm models, with the Langmuir and Redlich–Peterson models affording the best fit to the adsorption data. The adsorption was best described by a pseudo-second-order kinetics model and thermodynamically favored the endothermic chemisorption process. These results indicated the potential of S-MSN as an effective new adsorbent for dye adsorption.

Received 3rd July 2015
Accepted 18th August 2015

DOI: 10.1039/c5ra12931a

www.rsc.org/advances

1. Introduction

Dyes are the side products from various manufacturing industries and are considered as dangerous organic pollutants to the environment. Once these organics enter the water, they become more stable and more difficult to biodegrade, owing to their complex chemical structures.[1] Thus, removal of dyes from effluents is important and various physical, chemical, and biological dye elimination techniques have been developed.[2] However, the former has been shown to be the more effective method, which could overcome all of the problems associated with cost, secondary pollution, complexity, the large areas and the fact that it is time consuming. Among the physical techniques, adsorption is currently popular, but important for efficient dye removal, and all researchers desire an adsorbent that possesses a high adsorption capacity. This property is partly related to the surface area, pore volume, and porosity of adsorbents.

Recently, carbon nanotubes (CNTs) have attracted much attention in nanoscale science and technology, owing to their unique optical, electronic, and mechanical properties.[3,4] In addition to their similar properties with the most other popular adsorbents, activated carbon had also been used in the adsorption of various synthetic organic compounds.[5,6] However, owing to strong van der Waals forces along the length axis, CNTs are likely to aggregate and form bundles, making it difficult to disperse them homogeneously in various solvents, greatly limiting their applications.[7] Aggregation reduces the CNT surface area, especially for single-walled carbon nanotubes (SWCNTs), and it increases the difficulty in examining the already complex adsorption interactions between them and organic compounds. Thus, extensive research is focused on the surface modification of CNTs, mainly to enhance their compatibility and dissolution properties. Hybridization with other materials such as chitosan, graphene, and cellulose has been reported to enhance their dispersion properties and adsorption capacities.[8–10] However, coating CNTs with poly(sodium-4-styrenesulfonate), alumina, TiO_2, and silica layer is another technique that can overcome such problems, because these materials offer superior characteristics with a high specific surface area, high ordering, as well as a narrow pore-size distribution that makes them ideal adsorbents.[11–15] Recently, we also revealed the preparation of mesostructured silica nanoparticles (MSNs) coated onto MWCNTs, which resulted in efficient adsorption towards methylene blue (MB) dye.[4]

[a]*Centre of Hydrogen Energy, Institute of Future Energy, Universiti Teknologi Malaysia, 81310 UTM Johor Bahru, Johor, Malaysia. E-mail: aishah@cheme.utm.my*

[b]*Department of Chemical Engineering, Faculty of Chemical Engineering, Universiti Teknologi Malaysia, 81310 UTM Johor Bahru, Johor, Malaysia*

[c]*Department of Chemistry, Faculty of Science, Universiti Teknologi Malaysia, 81310 UTM Johor Bahru, Johor, Malaysia*

[d]*Department of Chemistry, Faculty of Mathematics and Natural Sciences, Institut Teknologi Sepuluh Nopember, Surabaya, 60111 Indonesia*

† Electronic supplementary information (ESI) available. See DOI: 10.1039/c5ra12931a

Indeed, the MSNs possess a large surface area, tunable pore size, and excellent dispersibility in aqueous media that leads to a high adsorption capacity.[16] Further modification using MSNs for highly adsorptive adsorbents would be beneficial. In addition, MWCNTs have been widely investigated, but only a few studies have focused on SWCNT-based adsorbents, although, on occasion, the latter has shown a better upshot.[17] Therefore, in this study, MSNs were hybridized with SWCNTs and the performance of the resulting adsorbent toward the adsorption of MB was investigated. Significantly, the characterization results show that the physico-chemical properties of the composite were improved, with interesting structure and high adsorptivity compared to the previous MSN/MWCNT composite that was prepared by the same procedure. The equilibrium, kinetics, and thermodynamics of adsorption were also studied in order to describe the process.

2. Experimental

2.1 Materials

Cetyltrimethylammonium bromide (CTAB), ethylene glycol (EG), tetraethyl orthosilicate (TEOS), methylene blue (MB), and 3-aminopropyl triethoxysilane (APTES) were purchased from Merck Sdn. Bhd., Malaysia. Ammonium hydroxide solution (NH_4OH) was obtained from QRec, Malaysia. Single walled carbon nanotubes (SWCNT) with diameter of 10–20 nm and length of 10–50 μm was purchased from Chengdu Organic Chemicals Co. Ltd., Chinese Academy of Sciences. All of the chemicals were used as received without further treatment.

2.2 Synthesis of pristine MSN and SWCNT-MSN composites

Mesostructured silica nanoparticles (MSN) sample was prepared by co-condensation and sol–gel method according to previous method.[18] Typically, CTAB surfactant, EG solvent and NH_4OH solution were dissolved in 700 mL of water with the following mole composition, respectively: 0.0032 : 0.2 : 0.2 : 0.1. After vigorous stirring with heating, 1.2 mmol TEOS and 1 mmol APTES were added to the clear mixture to give a white suspension solution. This solution was then stirred for another 2 h, and the samples were collected by centrifugation. The synthesized MSN were dried at 333 K and calcined at 823 K for 3 h to remove the surfactant.

The SWCNT and MSN composites (S-MSN) were prepared using the synthesis method of MSN with the addition of SWCNT at an early stage. Three different amount of CNTs (1, 3, and 5 wt%) were loaded to the mixture of CTAB surfactant, EG, NH_4OH solution and distilled water, and the composites obtained then denoted as 1S-MSN, 3S-MSN, and 5S-MSN, respectively. The mixture was stirred and heated at 323 K, TEOS was added, and then stirred for another 2 h. The samples were collected by centrifugation, dried at 333 K and calcined at 623 K for 3 h to remove the surfactant.

2.3 Characterization

The crystalline structure of samples were determined by X-ray diffraction (XRD) recorded on a Bruker AXS D8 X-ray powder diffractometer (CuKα radiation, $\lambda = 1.5418$ Å). Transmission electron microscopy (TEM) was carried out using a JEOL JEM-2100F microscope. The samples were ultrasonically dispersed in acetone and deposited on an amorphous and porous carbon grid. Field-emission scanning electron microscopy (using a JEOL JSM-6701F microscope with an accelerating voltage of 15 kV) was conducted to observe the topology of the samples. The samples were coated with platinum by electro-deposition under vacuum prior to analyses.

In this work, nitrogen physisorption was measured at 77 K using a Quantachrome Autosorb-1 analyzer. Prior to measurements, the samples were evacuated for 24 h at 573 K. Specific surface area (S_{BET}) values were calculated from the BET isotherm plots, in regions applicable to the derivation of the model between P/P_0 values of 0.05–0.3, while the total pore volume was determined from the uptake of nitrogen at a relative pressure of $P/P_0 \sim 0.99$ and pore size distributions were obtained by using the Density Functional Theory (DFT) method from the desorption isotherm.[19] FT-IR spectroscopy (using a Perkin Elmer Spectrum GX FTIR spectrometer) was performed to identify the chemical functional groups present in the samples. The substance was finely ground and dispersed into KBr powder-pressed pellets using a ratio of approximately 0.001 g sample/0.2 g KBr. IR absorbance data were obtained over a range of wavenumbers from 4000–400 cm^{-1}.

2.4 Adsorption study

The activity of the adsorbents was tested for the adsorption of MB. This was performed in batches consisting of MB solution at various concentrations (5–50 mg L^{-1}). The solution was stirred at room temperature and 300 rpm to uniformly disperse the adsorbent with a dosage (0.05–0.75 g L^{-1}). The desired pH of the dye solution was achieved *via* adjustment with 0.1 M HCl or 0.1 M NaOH. During the process, aliquots of 2 ml were withdrawn at pre-determined time intervals and centrifuged in a Hettich Zentrifugen Micro 120 before being analyzed by UV-Vis spectrophotometer (Agilent Technologies) to determine the residual concentration of MB. Each set of experiments was performed three times. The adsorption band of MB was taken at a maximum wavelength (λ_{max}) of 664 nm and the adsorption uptake, q_t (mg g^{-1}), of the adsorbent was calculated using the following equation:

$$q_t = \frac{(C_0 - C_t)V}{m} \quad (1)$$

where q_t is adsorption uptake at time t (mg g^{-1}), C_0 and C_t are the concentrations of MB at the initial time and at time t, respectively (mg L^{-1}), V (L) is the volume of the solution and m (g) is the mass of the S-MSN composite adsorbent used.

3. Results and discussion

3.1 Characteristics of the adsorbent materials

3.1.1 Crystallinity and morphological studies. Fig. 1 shows a low-angle powder XRD pattern in the range of $2\theta = 1.5$–10° for the 1S-MSN, 3S-MSN, and 5S-MSN materials. Three distinct diffraction peaks are observed at $2\theta = 2.35^\circ$, 4.10°, and 4.75°,

which are indexed as the (100), (110), and (200) reflections, respectively. This pattern is similar to that of pristine MSNs, with characteristic peaks of typical mesostructured silica materials with a *p6mm* 2D hexagonal structure.[4,18] A decrease in intensity of the peaks was observed with increasing amount of CNTs, demonstrating a decrease in the degree of crystallinity and mesopores uniformity in the MSNs.[20] However, the shapes of the three S-MSN composites peaks were preserved and no shift was observed, suggesting that there was no change in the lattice parameters of the composites. Thus, it is supposed that the CNTs somehow influence the crystallinity of the MSNs, but do not really alter the original structure and ordering of the MSNs.

The surface structure and morphology of the pristine MSN, 1S-MSN and 5S-MSN adsorbents were examined by FESEM and TEM, and the results are shown in Fig. 2. The results showed that the MSNs are spherical in shape, dangling off the CNTs like cluster of grapes, with an average particle size of 50 nm (Fig. 2B and C). The MSNs seemed to be compactly grown by increasing the amount of CNTs, creating larger particles size (Fig. 2D), signifying the role of the CNTs as a template for the growth of the MSNs.

3.1.2 Textural studies. The porosity of all of the adsorbents was studied by means of nitrogen adsorption–desorption (Fig. 3). The pore-size distributions of all adsorbents were analyzed by the non-local density functional theory (NLDFT) from the nitrogen adsorption branch.[21] As shown in Fig. 3A, all of the adsorbents exhibited type IV sorption isotherms with a H1 hysteresis loop, confirming a typical adsorption profile for a mesostructured material with highly uniform, open, and cylindrical pores.[22] It was seen that an increasing amount of CNTs in the MSNs reduced the volume of adsorbed nitrogen, implying a decrease in the orderliness of the MSN arrangements, in agreement with the decreased intensity of peak (100) in the low-angle XRD pattern in Fig. 1. 1S-MSN demonstrated two-step capillary condensation, with the first step at $P/P_0 = 0.3$, owing to intraparticle pores inside the MSNs, and the second step at a higher partial pressure ($P/P_0 = 0.9$), which was attributed to interparticle textural porosity. The intraparticle pores seemed almost eliminated when 3 and 5 wt% of CNTs were introduced into the MSNs, whereas the interparticle pores remained unchanged. This could be explained by pore blockage caused by the CNTs, as shown in the pore-size distribution in Fig. 3B, in which the primary pore size of approximately 3.2 nm in 1S-MSN decreased markedly, developing larger secondary pores at 5.0–9.3 nm.[23] Table 1 indicates the decrease in surface area and an increase in average pore size and pore volume with the increasing amount of CNTs in the MSNs. Taking into account the differences in textural properties of SWCNTs and MWCNTs, it is expected that the SWCNTs would present a higher adsorption capacity of MB than MWCNTs, because the specific surface area and total pore volume of SWCNTs are 233% and 107% higher than the respective values of MWCNTs.[18] It was also observed that MWCNTs have a higher average pore size compared to SWCNTs, which could be attributed to the aggregated pores present in MWCNTs.

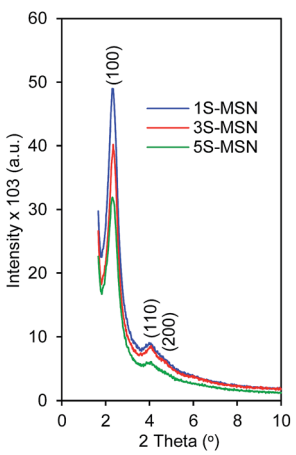

Fig. 1 XRD pattern of S-MSN.

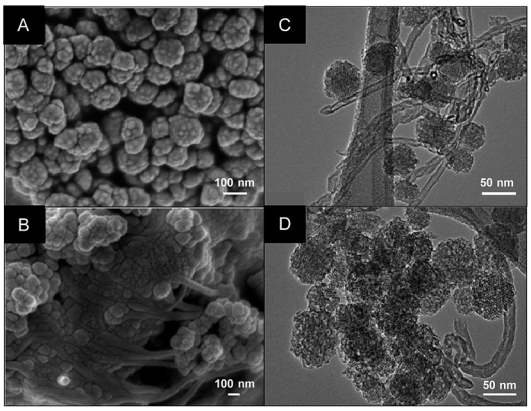

Fig. 2 FESEM images for (A) MSN (B) 5S-MSN and TEM images for (C) 1S-MSN and (D) 5S-MSN adsorbents.

3.1.3 Vibrational spectroscopy. The structural changes in S-MSNs were confirmed by FTIR analysis, and the results are shown in Fig. 4A. All of the adsorbents demonstrated similar FTIR spectra, with a typical pattern for mesoporous silica materials, consisting of bands at 3480, 1640, 1050, 960, 800, and 460 cm^{-1}, which were attributed to –OH stretching, water molecules retained by siliceous materials, Si–O–Si asymmetric stretching, external Si–OH groups, Si–O–Si symmetric stretching, and Si–O–Si bending, respectively.[18,24,25] For better observation, Fig. 4B summarizes the changes of all bands, based on the band intensities in pristine MSN. It could be seen that the increase in CNT loading onto MSNs intensified the Si–O–Si bonds at bands 1050 and 460 cm^{-1}, whereas it significantly decreased the band at 800 cm^{-1}, showing that the restructuring favored asymmetric and bending bonds rather than the symmetric bonds. The decrease in silanol groups with increasing amounts of CNTs, as shown at band 960 cm^{-1}, may explain the increase in Si–O–Si bonds, which most probably occur through dehydroxylation during calcination. Similar phenomena were observed in our previous study, in which Zn and/or Cu were loaded onto MSNs.[26] This observation is in agreement with decreases in the intensity of the XRD patterns as well as the surface area, verifying the role of CNTs in offering additional sites for silica growth.

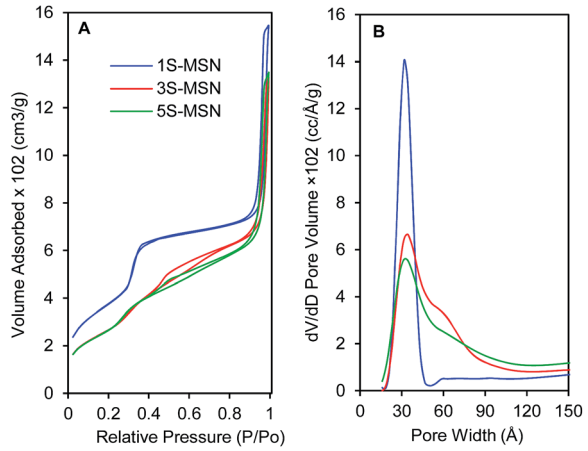

Fig. 3 (A) Nitrogen adsorption–desorption isotherms and (B) pore size distribution of S-MSN.

Table 1 Textural properties of adsorbents

Sample	Surface area, S_{BET} (m^2 g^{-1})	Average pore size (nm)	Pore volume, V_{pore} (cm^3 g^{-1})
MSN	1242	3.56	1.06
MWCNT	171	16.4	0.86
SWCNT	398	10.8	0.92
1S-MSN	1240	5.02	1.64
3S-MSN	997	6.96	1.81
5S-MSN	983	7.23	2.00

3.2 Mechanism of MSN formation on the surface of SWCNT

Based on the characterization results above, a mechanism for the formation of the CNT-MSN composite is proposed (Fig. 5). The higher concentration of CTAB surfactant around the CNT surface facilitated heterogeneous nucleation on the CNT surface, rather than a homogeneous one in the bulk solution.[27] This is most probably caused by a strong interaction through van der Waals forces of the CNTs with the hydrophobic end of CTAB.[28] When the concentration of the free surfactant molecules increased to the critical micelle concentration (CMC), free micelles formed on the outer surfaces of the CNTs.[29] Subsequently, calcination of the adsorbent at 623 K removed any CTAB or other organic compounds involved in the synthesis steps, while retaining the spherical-shaped MSNs on the surface of the CNTs. Significantly, it was found from this study that the interaction of CTAB with different type of CNTs produced different shaped CNT/MSN composites. Previously, the interaction of CTAB with MWCNTs produced a uniform mesoporous SiO_2 coating, whereas these SWCNTs gave grape-like SiO_2.[4] The detailed mechanism for both products is still under investigation, but the strength of van der Waals forces of the CNTs toward the CTAB seems to play an important role in promoting different SiO_2 growths around the CNT surface.[7] In addition, based on classical solid–liquid interface surfactant adsorption theory, an appropriate ratio of CTAB to CNTs also affected the uniformity of the SiO_2 growth.[30] A similar growth mechanism for a porous silica layer on SWCNTs and MWCNTs, with the aid of CTAB, has been reported previously.[29] Remarkably, this study brought new insight into the production of different shaped SiO_2 on CNTs, which is expected to enhance its adsorptivity towards adsorbate.

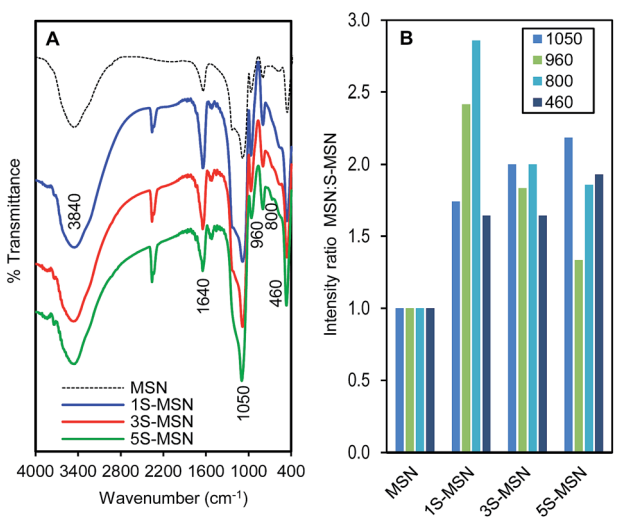

Fig. 4 (A) FTIR spectra for S-MSN and (B) summary of the related bands intensity.

3.3 Adsorption study

Next, the adsorptivity of both types of CNTs (5 wt% SWCNTs and MWCNTs) loaded onto MSNs was tested in terms of the adsorption of methylene blue (MB), and the results were compared with that of pristine MSN and SWCNT (Fig. 6A). It was observed that the SWCNT/MSN composite (S-MSN) adsorbed about three to five times more MB with 156 mg g^{-1} of adsorption capacity compared to MWCNT/MSN composite (M-MSN) (36 mg g^{-1}), pristine MSN (28 mg g^{-1}) and SWCNT (47 mg g^{-1}). Indeed, the higher surface area and average pore size of S-CNT plays an important role in this enhancement, confirming the advantage of the grape-like morphology of MSNs compared to the coating SiO_2.

An evaluation of the pH effect and adsorbent dosage showed that the adsorption was optimal at pH 7 with 0.05 g L^{-1} S-MSN (Fig. S1†). This can be described by the zero-point charge (pH_{ZPC}) of the adsorbent, which was determined to be at pH 6.0; thus, pH values above this strongly favored the adsorption of MB.[31] However, the lower the adsorbent dosage, the more the MB anions were adsorbed onto the surface per gram of S-MSN, resulting in a higher adsorption capacity (q_e).[32]

Fig. 6B shows the effect of SWCNT loading onto the MSNs, ranging from 1–5 wt%, at different adsorption temperatures. It can be seen, in all cases, that q_e increased with increasing CNT loading on the MSNs, which may be attributed to the increasing number of Si–O–Si bonds formed during the preparation process, which provide more adsorption sites for MB (Fig. 4). This result was supported by XRD, FTIR, and surface-area analyses, confirming the role of CNTs in boosting the silica growth. The abundant Si–O–Si bonds improved the porosity and

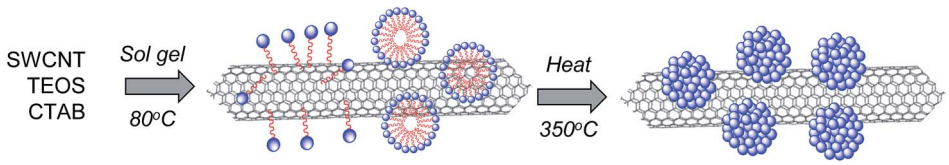

Fig. 5 Proposed mechanism for formation of S-MS.

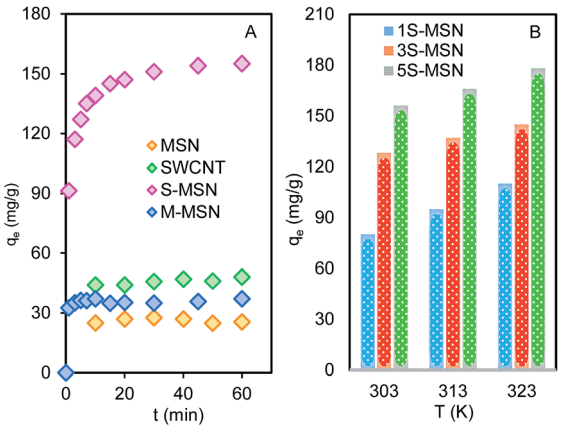

Fig. 6 Adsorption of MB by (A) MSN based adsorbents and (B) S-MSN under different SWCNT loading.

increased the surface area and pore size of S-MSN, which were important factors in enhancing the MB adsorption efficiency. While, the same trend in increasing q_e at all temperatures demonstrated the endothermic nature of the adsorption.

3.4 Equilibrium isotherm study

An adsorption isotherm describes the adsorption phenomenon regarding the mobility of dye molecules from an aqueous medium to an adsorbent at equilibrium at constant pH and temperature.[33] Herein, four available isotherm models, the Langmuir, Freundlich, Redlich–Peterson (R–P), and Dubinin–Radushkevich (D–R) models, were used for this purpose.[33–37] The nonlinear forms of these four isotherm models can be represented as follows:

$$\text{Langmuir}: q_e = \frac{q_m K_L C_e}{1 + K_L C_e} \quad (2)$$

$$\text{Freundlich}: q_e = K_F C_e^{1/n_F} \quad (3)$$

$$\text{Redlich} - \text{Peterson}: q_e = \frac{K_R C_e}{1 + a_R C_e^{b_R}} \quad (4)$$

$$\text{Dubinin–Radushkevich}: q_e = (q_m)\exp(-K_{DR}\varepsilon^2) \quad (5)$$

where q_e is the amount of MB adsorbed per gram of S-MSN adsorbent (mg g^{-1}), q_m is the maximum adsorption capacity obtained from the isotherm (mg g^{-1}), C_e is the concentration of MB at equilibrium (mg L^{-1}), n_F is a heterogeneity factor, a_R is the R–P isotherm constant, b_R is R–P isotherm exponent, R is the gas constant (8.314 J mol^{-1} K^{-1}), T is the absolute temperature (K), and K_L, K_F, K_R, and K_{DR} are the constants of the Langmuir, Freundlich, R–P, and D–R models, respectively.

The isotherm fittings for each model for the adsorption of MB onto S-MSN are shown in Fig. 7, whereas the extracted isotherm information is summarized in Table 2. Among the four isotherms tested, the Langmuir and R–P models were revealed to be the best models to describe the adsorption process, showing by the highest accuracy in terms of correlation coefficient (R^2). The good fitting observed with the Langmuir model suggests that the process follows a monolayer adsorption, in which there is no transmigration of the adsorbate on the surface plane.[34] A similar phenomenon has been observed in the adsorption of cationic dyes onto mesostructured silica materials.[4] However, all of the b_R values for the R–P model were higher than 1, signifying the strong adsorption capability to MB through heterogeneous predominated surface adsorption without the steric hindrance between the pores and adsorbate.[38]

The Freundlich and D–R isotherms could also be considered to explain the nature and mechanism of adsorption, based on their parameter values. In parallel with K_L in the Langmuir isotherm, all values of the Freundlich exponent n_F obtained in this study were also in the range of $0 < n_F > 1$, indicating favorable adsorption.[32] Furthermore, the mean sorption energy, E, in the D–R isotherm model was between 8 and 16 kJ mol^{-1}, representing a chemisorption process between the MB ions and S-MSN.[39]

3.5 Kinetics study

The adsorption kinetics were studied to determine the adsorbate uptake rate as well as the adsorption mechanism. Herein, the experimental data were fitted to three conventional kinetic models, namely, the Lagergren pseudo-first-order model, the Ho pseudo-second-order model, and the Weber and Morris intraparticle diffusion model.[40–42] The first two models are expressed as:

$$\text{Pseudo-first order}: q_t = q_e(1 - \exp^{-K_1 t}) \quad (6)$$

$$\text{Pseudo-second order}: q_t = \frac{K_2 q_e^2 t}{1 + K_2 q_e t} \quad (7)$$

where q_e is the equilibrium amount of dye adsorbed per gram of S-MSN (mg g^{-1}), q_t is the adsorption capacity obtained at time t (mg g^{-1}), t is the time interval (min), and K_1 and K_2 are the pseudo-first- (min^{-1}) and pseudo-second-order rate constants (mg g^{-1} min^{-1}), respectively.

Nonlinear plots of the pseudo-first- and pseudo-second-order kinetic models for the adsorption of MB onto S-MSN are

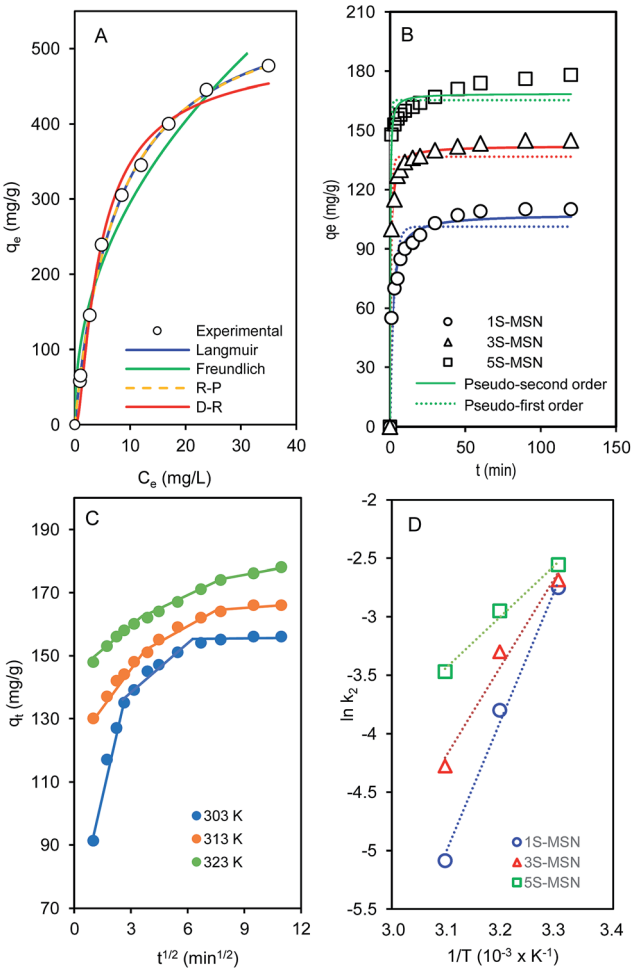

Fig. 7 (A) Non-linear plots of isotherm models (B) pseudo-first and second order kinetics models (C) Weber–Morris intraparticle diffusion and (D) activation energy.

shown in Fig. 7B, whereas their kinetic parameters and correlation coefficients are listed in Table 3. It can be seen from the figure that all experimental data from S-MSN fitted well with pseudo-second-order kinetics, and this was confirmed by the high value of R^2. In addition, the q_e values for the pseudo-second-order model were closer to the experimental data compared to the pseudo-first-order model. These kinetics results indicated that the adsorption occurred through a chemisorption process.[43] Similar adsorption characteristics have been reported for the adsorption of MB onto cellulose-based wastes, water hyacinth roots, and neem leaves.[41,44,45]

Next, the data were fitted with the intraparticle diffusion model to further investigate the possible mechanism and rate-controlling step of the adsorption. The equation is as follows:

$$\text{Intraparticle diffusion: } q_t = k_{id}t^{1/2} + C_i \quad (8)$$

where k_{id} is a constant of intraparticle diffusion (mg g^{-1} min$^{-1/2}$) and C_i is the thickness of the boundary layer. Plots of the amount of MB adsorbed (q_t) *versus* the square root of time ($t^{1/2}$) for 5 wt% S-MSN at different temperatures are shown in Fig. 7C. According to the Weber and Morris model, the q_t against $t^{1/2}$ plot should be linear, and if these lines pass through the origin, intraparticle diffusion is the only rate-controlling step.[32,46,47] It could be observed that none of the plots were linear over the entire time period, but could each be divided into three parts, demonstrating that three steps were involved in the adsorption process. These were (1) diffusion of MB towards S-MSN, (2) intraparticle diffusion of MB within the micro- and mesopores of S-MSN, and (3) diffusion through smaller pores, which was followed by the establishment of the equilibrium, because of the saturation of most of the adsorption sites.[48] The plot was approximately linear when the temperature was increased to 323 K, signifying the elimination of the faster initial and final steps, as a consequence of heat and agitation effects, leaving the intraparticle diffusion as a main step involved in the adsorption, but it was not the only rate-controlling step. The magnitude of C_i was found to increase

Table 2 Isotherm parameters for MB adsorption onto S-MSN

		SWCNT loading		
Isotherm	Parameters	1S-MSN	3S-MSN	5S-MSN
Langmuir	q_m (mg g^{-1})	323	336	478
	$K_L \times 10^{-1}$ (L mg^{-1})	2.35	2.06	1.27
	R^2	0.991	0.996	0.999
Freundlich	K_F	101	96.7	104
	n_F	2.83	2.66	2.21
	R^2	0.925	0.939	0.967
Redlich–Peterson	K_R	65.2	65.4	73.3
	$a^R \times 10^{-1}$	0.969	1.10	1.20
	q_m (mg g^{-1})	308	326	477
	b^R	1.18	1.13	1.01
	R^2	0.997	0.998	0.999
Dubinin–Radushkevich	q_m (mol g^{-1})	313	324	453
	$K_{DR} \times 10^{-3}$	1.07	1.16	1.57
	E (J mol^{-1})	21.6	20.8	17.8
	R^2	0.992	0.995	0.987

Table 3 Coefficient of pseudo-first and -second order adsorption kinetic models

			Pseudo-first-order			Pseudo-second-order		
CNT-MSN	T (K)	$q_{e,\ exp}$ (mg g^{-1})	$q_{e,\ cal}$ (mg g^{-1})	k_1 (min^{-1})	R^2	$q_{e,\ cal}$ (mg g^{-1})	$k_2 \times 10^{-2}$ (g mg^{-1} min^{-1})	R^2
1S-MSN	303	80	73.4	0.281	0.846	78.0	6.38	0.938
	313	95	92.2	0.171	0.969	101	0.224	0.959
	323	110	101	0.393	0.899	108	0.618	0.972
3S-MSN	303	128	120	0.511	0.919	127	6.83	0.982
	313	137	130	1.11	0.976	135	1.43	0.996
	323	145	137	1.18	0.962	142	1.39	0.993
5S-MSN	303	156	147	0.744	0.948	154	7.76	0.993
	313	166	154	1.80	0.955	159	2.05	0.979
	323	178	165	2.22	0.972	169	3.11	0.984

with increasing temperatures, equaling 88.1, 103.2, and 114.5 at 303, 313, and 323 K, respectively. This indicates that the thickness of the boundary layer of MB surrounded the S-MSN particles increased proportionally as a function temperature, which was a result of the increasing kinetic energy of MB, confirming the endothermic nature of the adsorption. A similar result was previously reported in terms of the dependence of temperature on the boundary layer for the adsorption of Pb(II) ions on China clay and Wollastonite.[49] This also verified that the adsorption is a chemisorption process.

The activation energy (E_a) is another important parameter in determining the type of adsorption. The magnitude of E_a gives information about whether the adsorption occurs mainly through physical or chemical adsorption processes.[50] The rate constant of the pseudo-second-order kinetic model, k_2 (listed in Table 4), was used to estimate the E_a of the adsorption of MB onto S-MSN using the Arrhenius equation in the way described below.

$$\ln k_2 = \ln A - \frac{E_a}{R}\left(\frac{1}{T}\right) \quad (9)$$

The slope of a linear plot of ln k_2 *versus* $1/T$ gave a value for E_a. A more positive energy reflects a greater energy required to initiate adsorption. In fact, low activation energies (5–40 kJ mol^{-1}) are characteristic of physisorption, whereas higher activation energies (40–800 kJ mol^{-1}) are recommended for chemical adsorption.[51] The plots for the E_a values are shown in Fig. 7D, and their values are summarized in Table 4. It can clearly be observed that 1S-MSN and 3S-MSN fell in the latter range, confirming the chemisorptive nature of the adsorption. However, a slightly lower E_a was observed for 5S-MSN, which may be attributed to abundant spherical MSNs dangling from the SWCNTs, which provide more adsorption sites for MB.

3.6 Thermodynamics study

In order to gain additional insight into the mechanism involved in the adsorption process, thermodynamic parameters for the present system were also calculated. Experiments were conducted at 303, 313, and 323 K for all adsorbents. The adsorption enthalpy (ΔH°), entropy (ΔS°), and Gibbs free energy (ΔG°) were calculated using the following thermodynamic functions:

$$\ln K_c = \frac{\Delta S^0}{R} - \frac{\Delta H^0}{RT} \quad (10)$$

$$K_c = \frac{C_e(\text{adsorbent})}{C_e(\text{solutiont})} \quad (11)$$

$$\Delta G^\circ = -RT \ln K_c \quad (12)$$

The linear form of the van't Hoff equation (eqn (10)) was plotted (figure not shown) to calculate values of ΔH° (kJ mol^{-1}) and ΔS° (J mol^{-1} K^{-1}) for the adsorption from the slope and intercept of ln K_c *versus* $1/T$, respectively. The thermodynamic parameters at three different temperatures are presented in Table 4. The positive ΔH° value confirmed the endothermic

Table 4 Thermodynamics parameters for the adsorption of S-MSN composites

CNT-MSN	T (K)	q_e (mg g^{-1})	ΔG° (kJ mol^{-1})	ΔH° (kJ mol^{-1})	ΔS° (J mol^{-1} K^{-1})	E_a (kJ mol^{-1})
1S-MSN	303	80	0.641	29.5	94.7	94.8
	313	95	0.190			
	323	110	−1.27			
3S-MSN	303	128	−1.11	46.3	157	64.6
	313	137	−3.35			
	323	145	−4.23			
5S-MSN	303	156	−1.83	41.2	143	39.1
	313	166	−3.73			
	323	178	−4.66			

nature of the adsorption, which was in agreement with the chemisorption process result obtained from the isotherm and kinetics studies.[48] Meanwhile, the positive value of ΔS° suggests an increase in randomness at the solid-solution interface during the adsorption of MB from aqueous solution onto S-MSN, which demonstrated a higher affinity of MB towards S-MSN.[52] The overall ΔG° value during the adsorption was negative for the range of temperatures investigated, which increased in magnitude as the temperature increased. This may correspond to an increase in the degree of spontaneity at elevated temperatures.

Therefore, the thermodynamic equilibrium isotherm and kinetics studies all verified that the adsorption of MB onto S-MSN composites occurred through a chemisorption process. It can be concluded that the adsorption takes place in an adsorbate–adsorbent system and it certainly depends upon the reactivity of the surface, the nature of the adsorbate and adsorbent, as well as the temperature of adsorption.

4. Conclusion

In this study, SWCNTs were loaded onto MSNs and successfully used as an adsorbent (S-MSN) in the enhanced adsorption of MB dye. The spherical-shaped MSNs that dangle from the SWCNTs like cluster of grapes provided a new insight into the previously reported study on MSNs coated uniformly on the surface of MWCNTs. It seemed that the interaction of CTAB with different types of CNTs produced different CNT/MSN shapes. The detailed mechanism for both products is still under investigation, but apparently the strength of the van der Waals forces of both types of CNTs towards CTAB, as well as the ratio of CTAB to CNTs, may play important roles in promoting different MS growths around the CNT surfaces. The characterization results showed that the growth of the MSNs became intense with the increasing CNT loading, which enhanced the adsorption sites for MB. As a result, 0.1 g L^{-1} 5S-MSN was able to adsorb 478 mg g^{-1} (q_m) of 50 mg L^{-1} MB at pH 7 and 323 K. The equilibrium data were evaluated using the Langmuir, Freundlich, Redlich–Peterson, and Dubinin–Radushkevich isotherm models, with the Langmuir and Redlich–Peterson models affording the best fit to the adsorption data. The adsorption was best described by the pseudo-second-order kinetics model and thermodynamically favored endothermic chemisorption process. These results indicate the potential of S-MSN composites as effective new adsorbents for dye adsorption.

Acknowledgements

The authors are grateful for the financial supports by the Research University Grant from Universiti Teknologi Malaysia (Grant No. 07H06) and the award of my PhD Scholarship (Ainul Hakimah Karim) from the Ministry of Higher Education Malaysia.

References

1 E. Forgacs, T. Cserháti and G. Oros, *Environ. Int.*, 2004, **30**, 953.
2 A. Siddiq, A. Shahid and R. Gill, *J. Environ. Chem. Eng.*, 2015, **3**, 892.
3 D. Eder, *Chem. Rev.*, 2010, **110**, 1348.
4 A. H. Karim, A. A. Jalil, S. Triwahyono, N. H. N. Kamarudin and A. Ripin, *J. Colloid Interface Sci.*, 2014, **421**, 93.
5 K. Yang, X. Wang, L. Zhu and B. Xing, *Environ. Sci. Technol.*, 2006, **40**, 5804.
6 X. Wang, S. Tao and B. Xing, *Environ. Sci. Technol.*, 2009, **43**, 6214.
7 B. Krause, M. Mende, P. Potschke and G. Petzold, *Carbon*, 2010, **48**, 2746.
8 S. Chatterjee and M. W. Lee, *Bioresour. Technol.*, 2010, **101**, 1800.
9 L. Ai and J. Jiang, *Chem. Eng. J.*, 2012, **192**, 156.
10 C. Deng, J. Liu, W. Zhou, Y. K. Zhang, K. F. Du and Z. M. Zhao, *Chem. Eng. J.*, 2012, **200**, 452.
11 Z. Y. Zhang and X. C. Xu, *Chem. Eng. J.*, 2014, **256**, 85.
12 V. K. Gupta, S. Agarwal and T. A. Saleh, *J. Hazard. Mater.*, 2011, **185**, 17.
13 J. Y. Jung, D. Lee and Y. S. Lee, *J. Alloys Compd.*, 2015, **622**, 651.
14 A. Siddiqa, A. Shahid and R. Gill, *J. Environ. Chem. Eng.*, 2015, **3**, 892.
15 J. Gong, J. Liu, Z. Jiang, X. Wena, E. Mijowska, T. Tang and X. Chen, *J. Colloid Interface Sci.*, 2015, **445**, 195.
16 S. M. Sidik, A. A. Jalil, S. Triwahyono, T. A. T. Abdullah and A. Ripin, *RSC Adv.*, 2015, **5**, 37405.
17 V. Georgakilas, D. Gournis, V. Tzitzios, L. Pasquato, D. M. Guldi and M. Pratod, *J. Mater. Chem.*, 2007, **17**, 2679.
18 A. H. Karim, A. A. Jalil, S. Triwahyono, S. M. Sidik, N. H. N. Kamarudin, R. Jusoh, N. W. C. Jusoh and B. H. Hameed, *J. Colloid Interface Sci.*, 2012, **386**, 307.
19 S. Brunauer, P. H. Emmett and E. Teller, *J. Am. Chem. Soc.*, 1938, **60**, 309.
20 K. C. Kao and C. Y. Mou, *Microporous Mesoporous Mater.*, 2013, **169**, 7.
21 J. Zhang, X. Li, J. M. Rosenholm and H. C. Gu, *J. Colloid Interface Sci.*, 2011, **361**, 16.
22 C. T. Kresge, M. E. Leonowicz, W. J. Roth, J. C. Vartuli and J. S. Beck, *Nature*, 1992, **359**, 710.
23 W. Zeng, Z. Wang, X. F. Qian, J. Yin and Z. K. Zhu, *Mater. Res. Bull.*, 2006, **41**, 1155.
24 N. H. N. Kamarudin, A. A. Jalil, S. Triwahyono, M. R. Sazegar, S. Hamdan, S. Baba and A. Ahmad, *RSC Adv.*, 2015, **5**, 30023.
25 N. H. N. Kamarudin, A. A. Jalil, S. Triwahyono, N. F. M. Salleh, A. H. Karim, R. R. Mukti, B. H. Hameed and A. Ahmad, *Microporous Mesoporous Mater.*, 2013, **180**, 235.
26 N. W. C. Jusoh, A. A. Jalil, S. Triwahyono and C. R. Mamat, *Appl. Catal., A*, 2015, **492**, 169.
27 I. Gorelikov and N. Matsuura, *Nano Lett.*, 2007, **8**, 369.
28 Y. Wan and D. Zhao, *Chem. Rev.*, 2007, **107**, 2821.
29 K. Ding, B. Hu, Y. Xie, G. An, R. Tao, H. Zhang and Z. Liu, *J. Mater. Chem.*, 2009, **19**, 3725.
30 S. Paria and K. C. Khilar, *Adv. Colloid Interface Sci.*, 2004, **110**, 75.
31 N. W. C. Jusoh, A. A. Jalil, S. Triwahyono, A. H. Karim, N. F. M. Salleh, N. H. R. Annuar, N. F. Jaafar,

M. L. Firmansyah, R. R. Mukti and M. W. Ali, *Appl. Surf. Sci.*, 2015, **330**, 10.
32 A. A. Jalil, S. Triwahyono, S. H. Adam, N. D. Rahim, M. A. A. Aziz, N. H. H. Hairom, N. A. M. Razali, M. A. Z. Abidin and M. K. A. Mohamadiah, *J. Hazard. Mater.*, 2010, **181**, 755.
33 I. Langmuir, *J. Am. Chem. Soc.*, 1917, **39**, 1848.
34 S. Banerjee, R. K. Gautam, A. Jaiswal, M. C. Chattopadhyaya and Y. C. Sharma, *RSC Adv.*, 2015, **5**, 14425.
35 Y. S. Ho, J. F. Porter and G. Mckay, *Water, Air, Soil Pollut.*, 2002, **141**, 1.
36 M. M. Dubinin and L. V. Radushkevich, *Proc. Acad. Sci., USSR*, 1947, **55**, 331.
37 F. C. Wu, B. L. Liu, K. T. Wu and R. L. Tseng, *Chem. Eng. J.*, 2010, **162**, 21.
38 P. D. Saha, S. Chakraborty and S. Chowdhury, *Colloids Surf., B*, 2012, **92**, 262.
39 S. Lagergren, *K. Sven. Vetenskapsakad. Handl.*, 1898, **24**, 1.
40 Y. S. Ho and G. McKay, *Process Biochem.*, 1999, **34**, 451.
41 W. J. Weber, J. C. Morris and J. Sanit, *J. Eng. Mech. Div., Am. Soc. Civ. Eng.*, 1963, **89**, 31.
42 S. M. Sidik, A. A. Jalil, S. Triwahyono, S. H. Adam, M. A. H. Satar and B. H. Hameed, *Chem. Eng. J.*, 2012, **203**, 9.
43 G. Annadurai, R. S. Juang and D. J. Lee, *J. Hazard. Mater.*, 2002, **92**, 263.
44 K. S. Low, C. K. Lee and K. K. Tan, *Bioresour. Technol.*, 1995, **52**, 79.
45 K. G. Bhattacharyya and A. Sharma, *Dyes Pigm.*, 2005, **65**, 51.
46 S. H. Adam, A. A. Jalil and S. Triwahyono, *Desalin. Water Treat.*, 2012, **49**, 337.
47 N. Salamun, S. Triwahyono, A. A. Jalil, T. Matsuura and N. F. M. Salleh, *RSC Adv.*, 2015, **5**, 14129.
48 M. A. Z. Abidin, A. A. Jalil, S. Triwahyono, S. H. Adam and N. H. N. Kamarudin, *Biochem. Eng. J.*, 2011, **54**, 124.
49 K. P. Yadava, B. S. Tyagi and V. N. Singh, *J. Chem. Technol. Biotechnol.*, 1991, **51**, 47.
50 H. Nollet, M. Roels and P. Lutgen, *Chemosphere*, 2003, **53**, 655.
51 B. Pan, P. Huang, M. Wu, Z. Wang, P. Wang, X. Jiao and B. Xing, *Bioresour. Technol.*, 2012, **103**, 367.
52 N. F. M. Salleh, A. A. Jalil, S. Triwahyono, J. Effendi, R. R. Mukti and B. H. Hameed, *Appl. Surf. Sci.*, 2015, **349**, 485.